

# A Quantum Repeater Platform based on Single SiV<sup>-</sup> Centers in Diamond with Cavity-Assisted, All-Optical Spin Access and Fast Coherent Driving

Gregor Bayer,<sup>1,\*</sup> Robert Berghaus,<sup>1,\*</sup> Selene Sachero,<sup>1</sup> Andrea B. Filipovski,<sup>1</sup> Lukas Antoniuk,<sup>1</sup> Niklas Lettner,<sup>1,2</sup> Richard Waltrich,<sup>1</sup> Marco Klotz,<sup>1</sup> Patrick Maier,<sup>1</sup> Viatcheslav Agafonov,<sup>3</sup> and Alexander Kubanek<sup>1,2,†</sup>

<sup>1</sup>*Institute for Quantum Optics, Ulm University, Albert-Einstein-Allee 11, 89081 Ulm, Germany*

<sup>2</sup>*Center for Integrated Quantum Science and Technology (IQst),  
Ulm University, Albert-Einstein-Allee 11, 89081 Ulm, Germany*

<sup>3</sup>*GREMAN, UMR 7347 CNRS, INSA-CVL, Tours University, 37200 Tours, France*

Quantum key distribution enables secure communication based on the principles of quantum mechanics. The distance in fiber-based quantum communication is limited to about a hundred kilometers due to signal attenuation. Thus, quantum repeaters are required to establish large-scale quantum networks. Ideal quantum repeater nodes possess a quantum memory which is efficiently connected to photons, the carrier of quantum information. Color centers in diamond and, in particular, the negatively-charged silicon-vacancy centers are promising candidates to establish such nodes. The major obstacle is an inefficient connection between the color centers spin to the Gaussian optics of fiber networks. Here, we present an efficient spin-photon interface. Individual silicon-vacancy centers coupled to the mode of a hemispherical Fabry-Pérot microcavity show Purcell-factors larger than 1 when operated in a bath of liquid Helium. We demonstrate coherent optical driving with a Rabi frequency of 290 MHz and all-optical access to the electron spin in strong magnetic fields of up to 3.2 T. Spin initialization within 67 ns with a fidelity of 80 % and a lifetime of 350 ns are reached inside the cavity. The spin-photon interface is passively stable, enabled by placing a color center containing nanodiamond in the hemispherical Fabry-Pérot mirror structure and by choosing short cavity lengths. Therefore, our demonstration opens the way to realize quantum repeater applications.

## I. INTRODUCTION

With the development of quantum computers new encryption methods become necessary to enable secure communication. Quantum key distribution (QKD) guarantees security based on the principles of quantum mechanics, where any eavesdropping attempt leaves an unavoidable fingerprint on the transmitted data [1, 2]. Photonic entanglement distribution among remote quantum nodes is the key element for quantum information exchange over long distances [3]. Fiber-based quantum channels are desirable for practical use, building on existing network technology, but are vulnerable to losses, which limits the distance for point-to-point links to about 100 km. Currently, the most promising way to establish long-distance quantum communication, without the need for trusted nodes, is based on modular quantum repeaters [4]. Experimental realizations of quantum repeaters are extremely difficult and subject to ongoing research efforts [5, 6]. The major experimental challenge is to develop elementary quantum repeater nodes with efficient fiber connectivity and, at the same time, access to long-lived quantum memories in order to reach transmission rates and state transfer fidelities that enable practical use over long distance. Recently, first demonstrations of quantum repeater nodes which contain necessary elements were demonstrated based on diamond technology [7].

Color centers in diamond are among the most promising platforms to realize quantum repeater nodes [8–11]. Pioneering work was done with negatively-charged nitrogen-vacancy (NV<sup>-</sup>) centers. A recent breakthrough marks the implementation of quantum network protocols in three-node entanglement-based quantum networks [12], where two-node entangled Bell state fidelity reaches 80 % with entangling rates about 9 Hz. Three-node heralded GHZ-state preparation reaches a state fidelity of 53.8 % and entanglement swapping across three nodes 58.7 % with rates of 25 mHz [12]. While all quantum repeater elements are established [13, 14], scaling to multiple nodes for long distances requires significant improvements. In particular, coherent photon emission and detection requires higher efficiency in order to maintain entanglement fidelity over long-distance links at high rates. A solution are spin-photon interfaces with Purcell-enhanced coherent photon interaction. Therefore, the optical transition of the NV<sup>-</sup> center can, for example, be coupled to the mode of a Fabry-Pérot (FP) microcavity [15–17]. Group IV color centers and, in particular, the negatively-charged silicon-vacancy (SiV<sup>-</sup>) center, are an attractive alternative to NV<sup>-</sup> centers. The D<sub>3d</sub> symmetry enables spectrally stable, optical transitions and indistinguishable photons without Stark tuning [18]. High brightness and large Debye-Waller factor lead to an intrinsically higher rate of coherent photon exchange. Its electron spin coherence time reaches 13 ms at mK-temperatures [19] and access to nuclear spins [20] potentially enables second-long memory times. But building an efficient spin-photon interface mode-matched to Gaussian optics still remains an outstanding challenge. Fast coherent op-

\* These two authors contributed equally

† Corresponding author; alexander.kubanek@uni-ulm.de

tical manipulation is blocked by inefficient light-matter interaction due to the high refractive index of the diamond host. Also, the need to operate at sub-Kelvin temperatures for long spin-coherence times requires dilution refrigerators raising technical demands.

As a solution, we propose to work with  $\text{SiV}^-$  centers in nanodiamonds (NDs) coupled to the mode of an optical FP microcavity. A locally modified phonon density of states (pDOS) could increase the operation temperature to few Kelvin, when the  $\text{SiV}^-$  center is localized inside a ND [21] making dilution refrigerators redundant. At the same time, the small size of NDs, smaller than the optical wavelength, enables integration into open resonators with low scattering loss [15, 22–24]. Therefore,  $\text{SiV}^-$  centers in NDs with their optical transitions coupled to the mode of an optical resonator are a promising spin-photon interface for quantum repeater applications.

In pioneering experiments,  $\text{SiV}^-$  centers in NDs [25] and in diamond membranes (DMs) [26] as well as germanium-vacancy ( $\text{GeV}^-$ ) centers in DMs [27] were coupled to the mode of fiber-based cavities at room temperature. Breakthroughs in the realization of stable FP cavities at cryogenic temperatures [28–36] enabled cavity coupling of  $\text{SiV}^-$  centers at low temperatures [37]. While integrated platforms for microwave control of the  $\text{NV}^-$  centers electron spin inside open FP microcavities are developed [38],  $\text{SiV}^-$  center electron spin access is yet to be demonstrated inside open resonators. At the same time, coherent optical driving and significant Purcell-enhancement that shortens the optical lifetime is required. All these elements are essential for an efficient quantum repeater node and need to be established simultaneously.

Here, we realize such a spin-photon interface by coupling individual optical transitions of single  $\text{SiV}^-$  centers in a ND to the mode of an open microcavity at cryogenic temperatures. We demonstrate coherent optical driving with Rabi frequencies of 290 MHz, significant lifetime shortening yielding Purcell-factors well above 1 and all-optical, cavity-assisted electronic spin access in presence of a strong magnetic field. Therefore, we establish a promising platform to serve as a quantum repeater node which is passively stable and enables efficient mode-matching of the fundamental Gaussian TEM-mode to fiber networks.

## II. EXPERIMENTAL DETAILS

NDs with ingrown  $\text{SiV}^-$  centers are precharacterized using confocal spectroscopy, see SI. Promising NDs of small size and with spectrally stable  $\text{SiV}^-$  centers are placed in the curved mirror of the FP microcavity utilizing AFM-based pick-and-place technique [39, 40] (fig. 1 **a**), upper panel). The hemispherical cavity is optimized towards small mode volume,  $V$ , and high coupling strength. Therefore, a mirror with small radius of curvature  $\text{RoC} \approx 8 \mu\text{m}$  is fabricated using focused ion beam milling following recipes of pioneering work [41–43]. Dis-

tributed Bragg reflectors (DBRs) are coated with symmetric reflectivities on both mirrors. The transmission  $T = 500$  ppm at wavelength  $\lambda = 737$  nm corresponds to a coating-limited Finesse of  $\mathcal{F}_{\text{ideal}} \approx 6300$ , see SI. After the ND-placement, the assembled ND - FP microcavity system reaches a Finesse of  $\mathcal{F} = 2700 \pm 500$  including all residual losses, such as scattering on the air-diamond interface. We optimize the system towards high passive stability by comprising moderate Finesse and a small mode volume resulting in reasonable high quality factor  $Q$ . Thereby, we avoid the high demands on mechanical stability and advanced locking of high-Finesse open cavities [33]. Furthermore, we operate the open-cavity directly in a liquid He-bath providing, in principle, infinite cooling power.

Positioning the ND in the center of the concave mirror enables highly accurate alignment of the  $\text{SiV}^-$  center to the FP microcavity mode and bears the advantage of a fixed emitter-cavity coupling without the need to scan the plane mirror in  $xy$ -directions. Spectral overlap can be optimized in-situ by tuning the cavity length in  $z$ -direction. A subsequent AFM scan verifies the successful transfer of the ND to the center of the curved mirror (fig. 1 **a**), lower panel). The size of the ND yields 300 nm in lateral dimensions and 200 nm in height. The  $\text{SiV}^-$  center is then resonantly excited via the fundamental  $\text{TEM}_{00}$ -mode of order  $n$  with laser light at a wavelength of  $\lambda_{\text{las}} \approx 736.7$  nm. Mode  $n - 1$  is located at longer wavelength and couples to the phonon sideband emission. The obtained emission spectra at 4 K are shown in fig. 1 **b**) (upper panel) for two different cavity lengths while keeping the same excitation wavelength  $\lambda_{\text{las}}$ . In the idealized case of a planar resonator the mode wavelength is given by  $\lambda_n = \frac{2}{n}L$ , where  $L$  describes the effective distance between the two mirrors. It follows that  $\frac{\lambda_{n-1}}{\lambda_n} = \frac{n}{(n-1)}$ . For the two cavity lengths with a difference  $\Delta L \approx \frac{3}{2}\lambda_{\text{las}}$  we find  $n = 8$  and  $n = 11$  in agreement with the value for  $\Delta L$ . Note, that the fundamental  $\text{TEM}_{00}$ -modes with orthogonal polarization are degenerate, enabling independent control of the light polarization.

A second order auto-correlation measurement yields  $g^{(2)}(0) = 0.33 \pm 0.06$  without background correction, shown in fig. 1 **b**) (lower panel), and proves single photon emission through the cavity modes under resonant excitation. Note, that two peaks marked in grey arise from reflected fluorescence signal in the detectors, which is resolved in later measurements, see SI.

When cooled in the liquid Helium bath, narrow spectral lines become apparent in the photoluminescence excitation (PLE) scans. Individual slightly power-broadened line scans reveal linewidths  $\gamma$  below 300 MHz as it would be expected for Fourier-transform (FT) limited lines for  $\text{SiV}^-$  centers (fig. 1 **c**)). Remarkably, the cavity-assisted PLE scans disclose a long-term stability, where individual line-scans differ less than the FT-limited linewidth on timescales of 90 s. Notably, the microcavity length is not actively stabilized throughout the scans. Instead, the mechanical stability arises from the passive stability

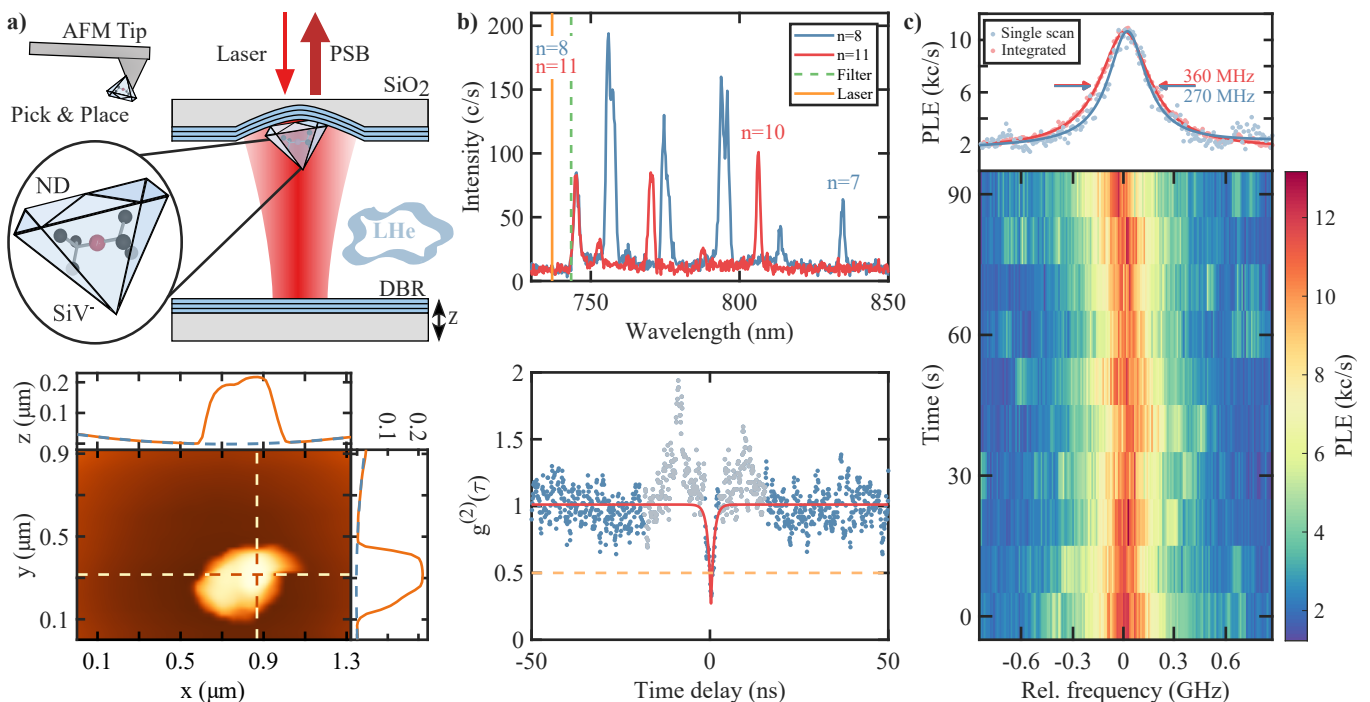


Figure 1. Assembling the coupled ND-microcavity system. **a)** A pre-characterized ND is picked with an AFM and placed in the hemispherical Fabry-Pérot mirror (upper panel). A subsequent AFM scan reveals the ND inside the mirror structure with a RoC of  $8\ \mu\text{m}$  indicated by blue-dashed lines (lower panel). **b)** Resonant PLE through the cavity mode yields  $\text{SiV}^-$ -sideband emission modulated by individual cavity modes shown for two different cavity lengths (upper panel). An auto-correlation measurement  $g^{(2)}(\tau)$  discloses single photon emission with  $g^{(2)}(0) < 0.5$  (lower panel). **c)** The power-broadened PLE linewidth below 300 MHz (scanning speed  $\approx 180\ \text{MHz s}^{-1}$ ) yields a long-term stability within  $\pm 12\ \text{MHz}$  over 90 seconds.

of the setup that persists even when operating in the liquid Helium bath. An estimation of the maximum length fluctuation yields that the microcavity length changes by less than one linewidth, corresponding to 160 pm, see SI.

### III. CAVITY-ENHANCED, COHERENT OPTICAL DRIVING OF INDIVIDUAL $\text{SiV}^-$ CENTERS

An optical transition on resonance with the cavity mode results in a modified spontaneous decay rate. The reduction of the excited state lifetime  $\tau$  is described by the Purcell-factor

$$F_P = \frac{\tau_{\text{free}}}{\tau_{\text{cav}}} = 1 + \xi f_P, \quad (1)$$

where  $\tau_{\text{free}}$  and  $\tau_{\text{cav}}$  are the emitter lifetimes in freespace and in the cavity respectively and  $\xi$  is the off-resonant branching ratio.  $f_P$  can be calculated as

$$f_P = \frac{3}{4\pi^2} \frac{\lambda^3 Q}{n^3 V} \quad (2)$$

with the light wavelength  $\lambda$  and the refractive index  $n$  of the medium inside the microcavity. For our system  $Q$  is primarily limited by the broader cavity resonances

$Q_{\text{emitter}} \approx 100 \times Q_{\text{cav}}$ . The fundamental cavity mode volume  $V = \frac{\pi}{4} L \omega_0^2$  is determined by Gaussian beam properties. With an emitter placed on the curved mirror,  $V$  deviates from a linear dependence on the cavity length  $L$ , see SI. Therefore, in contrast to the case of an emitter located on the flat side,  $F_P$  strongly depends on  $L$ , as shown in Table I for idealized cavity parameters, suggesting higher  $F_P$  for shorter lengths. In a real system, additional factors such as a limited quantum efficiency, branching ratio, dipole location and orientation need to be accounted for. For our system, the coupling is reduced by a factor of 1.58 as compared to an emitter located on the flat side but with aforementioned advantages for the assembled cavity system.

Table I. Microcavity parameters for two effective lengths. From RoC,  $L$  and  $\mathcal{F}$ , parameters such as  $Q$ ,  $V$ ,  $\omega_0$ , the ratio of beam waist on the curved to the flat side  $(\omega^{(L)}/\omega_0)^2$  and the respective Purcell-factors  $F_P^{\text{flat}}$  and  $F_P^{\text{curv}}$  are determined.

$n$	$L_{\text{eff}}\ (\mu\text{m})$	$Q$	$V\ (\lambda_{\text{las}}^3)$	$\omega_0\ (\mu\text{m})$	$(\omega^{(L)}/\omega_0)^2$	$F_P^{\text{flat}}$	$F_P^{\text{curv}}$
8	2.94	22000	5.2	0.95	1.58	980	620
11	4.05	30000	7.5	0.97	2.03	950	470

In the experiment, we choose the mode  $n = 8$  and study the saturation behaviour of the emitter as shown in fig. 2 a). Extracting to zero power yields a full

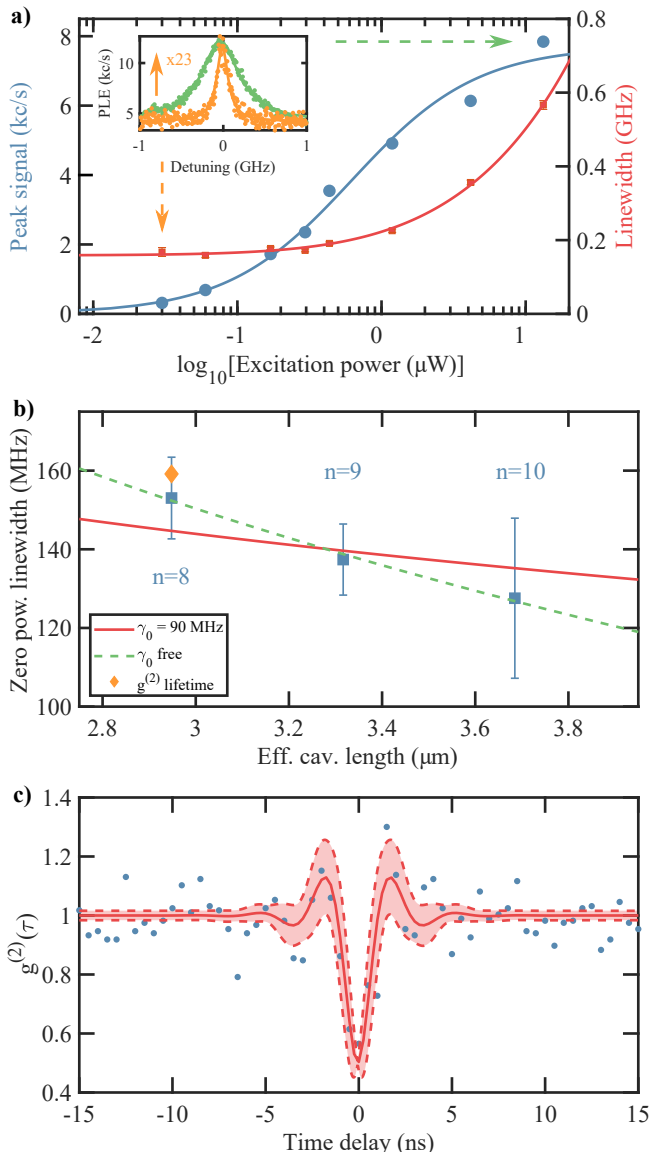


Figure 2. Purcell-enhancement and coherent optical driving. **a)** Peak count rates and linewidth from PLE scans with varying laser excitation power at the shortest accessible cavity mode  $n = 8$ . The linewidth extrapolated to zero power yields 168 MHz. The inset shows respective PLE scans for the highest and lowest (scaled by 23) optical power. **b)** Zero-power linewidth averaged for multiple measurements at three different cavity lengths. The Purcell-factor is extracted from fits with the freespace linewidth as a free parameter and fixed to 90 MHz. **c)** Resonant  $g^{(2)}(\tau)$ -measurement under strong drive reveal an optical lifetime of  $\tau = (1.0 \pm 0.5)$  ns and a Rabi frequency  $\Omega_R/2\pi = (290 \pm 50)$  MHz.

width at half maximum linewidth of 168 MHz. Repeating this measurement yields an averaged linewidth of  $(153 \pm 11)$  MHz (fig. 2 **b)**). For longer cavity lengths, the averaged linewidth reduces to  $(128 \pm 21)$  MHz with a minimal linewidth measured of 107 MHz. This suggests that the free-space emitter linewidth lies close to the FT-limit of  $\text{SiV}^-$  centers in the range 90 – 100 MHz. Assum-

ing a FT-limited emitter linewidth, the ratio shown in eq. (1) can be reformulated as

$$\frac{\gamma_{\text{cav}}}{\gamma_{\text{free}}} = \frac{\tau_{\text{free}}}{\tau_{\text{cav}}}. \quad (3)$$

The zero-power extracted linewidths for the  $\text{SiV}^-$  center coupled at different cavity lengths is fit with two different bounds, as shown in fig. 2 **b)**. A fit without any restriction on the averaged linewidth finds a free-space linewidth of 7 MHz, corresponding to a lifetime  $\tau_{\text{free}} = 23$  ns and a Purcell-factor of 21. Usually, excited state lifetimes of 1.5-2 ns are reported [18, 44]. Therefore, we also fit with the free-space linewidth fixed to 90 MHz, corresponding to  $\tau_{\text{free}} = 1.77$  ns, and extrapolate  $F_P = 1.61 \pm 0.06$ . The difference in the extrapolated Purcell-factors could arise from an increasing suppression of emission into the sideband as the effective cavity length shortens, as studied in detail for  $\text{NV}^-$  centers in [15]. Therefore, we assume our extracted Purcell-factor of 1.61 marks a lower bound.

A resonant, second-order auto-correlation measurement (fig. 2 **c)**) with high excitation power of  $7 \mu\text{W}$ , corresponding to a power-broadened linewidth of  $(433 \pm 8)$  MHz, reveals coherent optical driving of the system. The arising Rabi-oscillations are fit with a resonant  $g^{(2)}(\tau)$ -model, yielding an optical lifetime  $\tau = (1.0 \pm 0.5)$  ns and a Rabi-frequency  $\Omega_R/2\pi = (290 \pm 50)$  MHz.  $\tau = 1.0$  ns corresponds to a homogeneous linewidth of about 160 MHz (marked yellow in fig. 2 **b)**), in agreement with this cavity length.

The ideal Purcell-factor for our cavity could reach up to 530, see Table I. Deviations from the ideal case include low quantum efficiency (order of 0.05 [9]) and off-resonant branching ratio (0.325 [45]). An imperfect overlap of dipole and cavity field further reduces  $F_P$ .

The  $\beta$ -factor

$$\beta = \frac{F_P - 1}{F_P} \quad (4)$$

quantifies the fraction of excited state population, that decays through coherent coupling into the microcavity mode. With the extrapolated value of  $F_P = 1.61$ , we estimate  $\beta \approx 38\%$  as a lower bound.

#### IV. ALL-OPTICAL SPIN ACCESS

We now access the electronic spin state all-optically via the cavity mode. Therefore, we split the spin-orbit states by applying a magnetic field of variable strength and resonantly address the resulting spin-cycling transitions, labeled as  $C_2$  and  $C_3$  in fig. 3 **a)**. The cavity mode ( $n=8$ ) is on resonance with the  $\text{SiV}^-$  centers optical transition. PLE scans at magnetic fields of  $B=0$ , 2.1 and 3.2 T reveal the field-dependent splitting into the two spin-cycling transitions  $C_2$  and  $C_3$ , shown in fig. 3 **b)**. The splitting of the spin-conserving transition is a

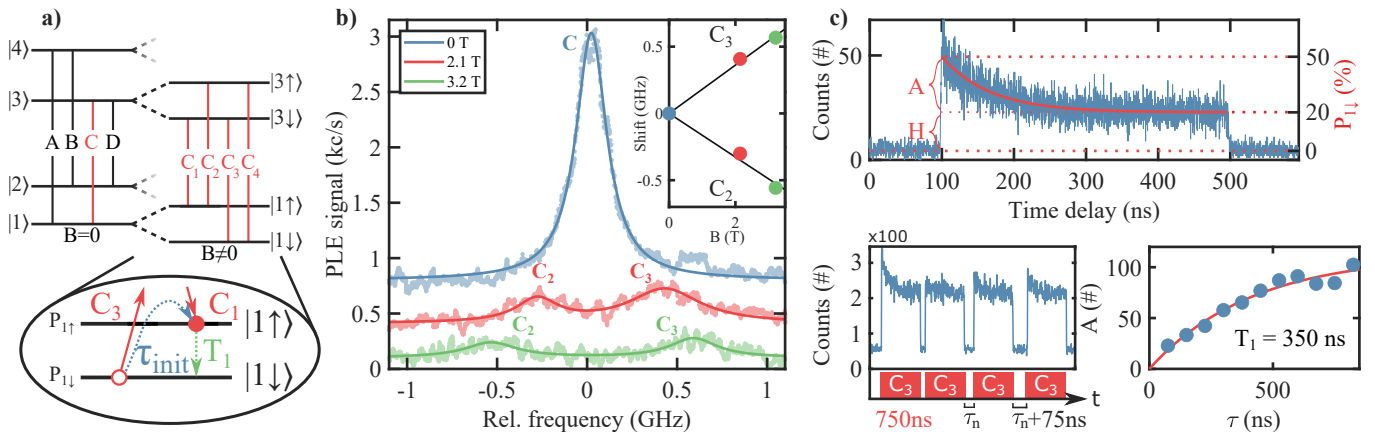


Figure 3. All-optical initialization of the  $\text{SiV}^-$  centers electron spin. **a)** Energy level diagram with and without external magnetic field applied along the cavity axis. In an external magnetic field the spin is initialized in the up-state by optical pumping on the spin-conserving transition  $C_3$ . **b)** The B-field dependent PLE signal shows the splitting of transition C into the spin-conserving transitions  $C_2$  and  $C_3$ . For better visibility the scans are offset by 0.4 kc/s. The inset shows the relative peak position over the field strength. **c)** When pumping on resonance with  $C_3$ , the exponential decay of the fluorescence signal indicates the initialization in the spin-up state (upper panel). A sequence of 750ns-long laser pulses separated by an increasing waiting time by increments of 75 ns yields the recovery into the equilibrium state (lower, left panel). The amplitude of an exponential fit to the decaying signal of every pulse is plotted against increasing waiting time (lower, right panel) revealing an electron spin lifetime of  $T_1^{\text{spin}} = (350 \pm 40)$  ns.

result of strain [46] and magnetic field alignment to the  $\text{SiV}^-$  center axis. We attribute the reducing brightness with increasing magnetic field to a prolonged lifetime of the electron spin state as compared to the lifetime of the orbital state. Consequently, optically pumping for the duration of the spin lifetime  $T_1^{\text{spin}}$  yields a reduced brightness.

In order to access the spin state at  $B = 3.2$  T, we apply 400 ns long laser pulses resonant to  $C_3$  at the relative frequency  $\Delta\nu \approx 0.6$  GHz, shown in fig. 3 c) (upper panel). The exponential fit to the fluorescence signal yields an initialization time  $\tau_{\text{init}} \approx (67 \pm 6)$  ns, on which the system is pumped into the spin-up state. The fidelity of the electron spin initialization is extracted to  $(80 \pm 4)\%$  by comparing the counts in the beginning and at the end of the pulse [47]. We assume, that the system is initially in an equal distribution of spin-up and spin-down. After optical pumping the system is preferably in spin-up state, decreasing the fluorescence signal on transition  $C_3$  accordingly, see SI. To determine the recovery time we vary the waiting time of consecutive 750 ns-long pulses with an increment of 75 ns, as depicted in fig. 3 c) (lower, left panel). An exponential fit on the fluorescence pulse heights yields a lifetime of  $T_1^{\text{spin}} = (350 \pm 40)$  ns, see fig. 3 c) (lower, right panel).  $T_1^{\text{spin}}$  is limited by mixing of the spin states due to non-perfect magnetic field alignment, which we can not precisely control in our setup. Furthermore, remaining strain fundamentally limits the achievable  $T_1^{\text{spin}}$ . The spin lifetime,  $T_1^{\text{spin}}$ , and initialization,  $\tau_{\text{init}}$ , are two competing processes on similar timescales in the initialization process. Therefore, we assume this to be the main limiting factor of the spin initialization fidelity. Note, that we did not observe the spin-flipping

transitions,  $C_1$  and  $C_4$  [47], which we attribute to reduced fluorescence in strong magnetic fields, making the usually weaker spin-flipping transitions hardly detectable.

Besides the application as quantum repeater node, our platform might prove valuable as sensor at high magnetic fields. From the fit accuracy of the B-field dependent splitting in fig. 3 b) we estimate a sensitivity of  $(180 \pm 60)$  mT Hz $^{-1/2}$  to determine dc-field strengths in high magnetic fields, here done at 3.2 T. For comparison, the  $\text{NV}^-$  center reach dc-magnetic field sensitivities of 40 nT Hz $^{-1/2}$ , seven orders of magnitude below the sensitivity of our system [48]. However, magnetometry with  $\text{NV}^-$  centers has limitations in high-field sensing. Typically, microwaves with frequencies on the order of 100 GHz are necessary in strong fields, requiring broadband tunable sources and compatible waveguides [49]. Instead, our system requires a tunable laser, thus keeping additional technical expenses low. In the future, the sensitivity can be enhanced by employing NDs with lower strain and by improving the B-field alignment.

## V. CONCLUSION AND OUTLOOK

Summarizing, we introduce a passively-stable quantum repeater platform based on single  $\text{SiV}^-$  center coupled to the mode of a FP microcavity. We coherently drive individual optical transitions through the cavity mode with a Rabi frequency of  $\Omega_R/2\pi = (290 \pm 50)$  MHz. The resulting lifetime shortening yields a Purcell-factor of 1.61 as lower bound. We further demonstrate all-optical, electron-spin initialization with an initialization time of  $\tau_{\text{init}} \approx 67$  ns and a fidelity of 80%. The observed spin

lifetime of  $T_1^{\text{spin}} = 350$  ns in a strong magnetic field of 3.2 T is limited by field misalignment.

With a well-aligned magnetic field, electron spin lifetimes in the ms-range and coherence times in the  $\mu$ s-range become feasible at liquid Helium temperatures [20]. Furthermore, access to nuclear spin opens the possibility for longer quantum storage times with coherence times well beyond millisecond timescales [19, 20]. In addition, by further optimizing coupling parameters and reducing scattering losses higher Purcell-factors are within reach. Increasing the Finesse to  $\mathcal{F} = 10.000$  ( $\mathcal{F} = 50.000$ ), photon extraction efficiencies of  $\beta = 69\%$  ( $\beta > 90\%$ ) and Purcell-factors above  $F_P = 3$  ( $F_P = 12$ ) are predicted for a short cavity length, see SI. Therefore, we believe this platform will be capable of tackling the two main obstacles for quantum repeater applications, namely low operation bandwidth and rapid quantum memory dephasing. Our work delivers experimental input to theoretical protocol developments [50, 51] towards high secret key transmission rates over long distances exceeding hundreds of

kilometers. Connecting many such quantum repeater nodes will overcome the limitations of direct quantum information transmission and lead to extended quantum networks.

### A. Acknowledgments

The authors thank V.A. Davydov for synthesis and processing of the nanodiamond material. The authors thank Jason Smith for fruitful discussions. The authors gratefully acknowledge the funding by the German Federal Ministry of Education and Research (BMBF) within the project Q.Link.X (16KIS0875) and QR.X (16KISQ006). The authors gratefully acknowledge the funding by the European Union and the DFG within the Quantero-project SensExtreme. A.K. and N.L. acknowledge support of IQst. Most measurements were performed on basis of the QuDi software suite [52].

- 
- [1] S. Pirandola, U. L. Andersen, L. Banchi, M. Berta, D. Bunandar, R. Colbeck, D. Englund, T. Gehring, C. Lupo, C. Ottaviani, J. L. Pereira, M. Razavi, J. Shamsul Shaari, M. Tomamichel, V. C. Usenko, G. Vallone, P. Villoresi, and P. Wallden, *Advances in quantum cryptography, Advances in Optics and Photonics* **12**, 1012 (2020).
- [2] V. Scarani, H. Bechmann-Pasquinucci, N. J. Cerf, M. Dušek, N. Lütkenhaus, and M. Peev, *The security of practical quantum key distribution, Reviews of Modern Physics* **81**, 1301 (2009).
- [3] S. Wehner, D. Elkouss, and R. Hanson, *Quantum internet: A vision for the road ahead, Science* **362**, eaam9288 (2018).
- [4] H.-J. Briegel, W. Dür, J. I. Cirac, and P. Zoller, *Quantum Repeaters: The Role of Imperfect Local Operations in Quantum Communication, Physical Review Letters* **81**, 5932 (1998).
- [5] N. Sangouard, C. Simon, H. de Riedmatten, and N. Gisin, *Quantum repeaters based on atomic ensembles and linear optics, Reviews of Modern Physics* **83**, 33 (2011).
- [6] S. Muralidharan, L. Li, J. Kim, N. Lütkenhaus, M. D. Lukin, and L. Jiang, *Optimal architectures for long distance quantum communication, Scientific Reports* **6**, 20463 (2016).
- [7] M. K. Bhaskar, R. Riedinger, B. Machielse, D. S. Levonian, C. T. Nguyen, E. N. Knall, H. Park, D. Englund, M. Lončar, D. D. Sukachev, and M. D. Lukin, *Experimental demonstration of memory-enhanced quantum communication, Nature* **580**, 60 (2020).
- [8] M. Ruf, N. H. Wan, H. Choi, D. Englund, and R. Hanson, *Quantum networks based on color centers in diamond, Journal of Applied Physics* **130**, 070901 (2021).
- [9] D. Chen, N. Zheludev, and W.-b. Gao, *Building Blocks for Quantum Network Based on Group-IV Split-Vacancy Centers in Diamond, Advanced Quantum Technologies* **3**, 1900069 (2020).
- [10] N. H. Wan, T.-J. Lu, K. C. Chen, M. P. Walsh, M. E. Trusheim, L. De Santis, E. A. Bersin, I. B. Harris, S. L. Mouradian, I. R. Christen, E. S. Bielejec, and D. Englund, *Large-scale integration of artificial atoms in hybrid photonic circuits, Nature* **583**, 226 (2020).
- [11] C. Bradac, W. Gao, J. Forneris, M. E. Trusheim, and I. Aharonovich, *Quantum nanophotonics with group IV defects in diamond, Nature Communications* **10**, 5625 (2019).
- [12] M. Pompili, S. L. N. Hermans, S. Baier, H. K. C. Beukers, P. C. Humphreys, R. N. Schouten, R. F. L. Vermeulen, M. J. Tiggelman, L. dos Santos Martins, B. Dirkse, S. Wehner, and R. Hanson, *Realization of a multinode quantum network of remote solid-state qubits, Science* **372**, 259 (2021).
- [13] F. Rozpędek, R. Yehia, K. Goodenough, M. Ruf, P. C. Humphreys, R. Hanson, S. Wehner, and D. Elkouss, *Near-term quantum-repeater experiments with nitrogen-vacancy centers: Overcoming the limitations of direct transmission, Physical Review A* **99**, 052330 (2019).
- [14] L. Kamin, E. Shchukin, F. Schmidt, and P. van Loock, *Exact rate analysis for quantum repeaters with imperfect memories and entanglement swapping as soon as possible (2022), arXiv:2203.10318 [quant-ph]*.
- [15] S. Johnson, P. R. Dolan, T. Grange, A. A. P. Trichet, G. Hornecker, Y. C. Chen, L. Weng, G. M. Hughes, A. A. R. Watt, A. Auffèves, and J. M. Smith, *Tunable cavity coupling of the zero phonon line of a nitrogen-vacancy defect in diamond, New Journal of Physics* **17**, 122003 (2015).
- [16] D. Riedel, I. Söllner, B. J. Shields, S. Starsielec, P. Appel, E. Neu, P. Maletinsky, and R. J. Warburton, *Deterministic Enhancement of Coherent Photon Generation from a Nitrogen-Vacancy Center in Ultrapure Diamond, Physical Review X* **7**, 031040 (2017).
- [17] M. Ruf, M. Weaver, S. van Dam, and R. Hanson, *Resonant Excitation and Purcell Enhancement of Coherent Nitrogen-Vacancy Centers Coupled to a Fabry-Perot Mi-*



- croavity, *Physical Review Applied* **15**, 024049 (2021).
- [18] L. Rogers, K. Jahnke, T. Teraji, L. Marseglia, C. Müller, B. Naydenov, H. Schauffert, C. Kranz, J. Isoya, L. McGuinness, and F. Jelezko, Multiple intrinsically identical single-photon emitters in the solid state, *Nature Communications* **5**, 4739 (2014).
- [19] D. D. Sukachev, A. Sipahigil, C. T. Nguyen, M. K. Bhaskar, R. E. Evans, F. Jelezko, and M. D. Lukin, Silicon-Vacancy Spin Qubit in Diamond: A Quantum Memory Exceeding 10 ms with Single-Shot State Readout, *Physical Review Letters* **119**, 223602 (2017).
- [20] M. H. Metsch, K. Senkalla, B. Tratzmiller, J. Scheuer, M. Kern, J. Achard, A. Tallaire, M. B. Plenio, P. Siyushev, and F. Jelezko, Initialization and Readout of Nuclear Spins via a Negatively Charged Silicon-Vacancy Center in Diamond, *Physical Review Letters* **122**, 190503 (2019).
- [21] M. Klotz, K. G. Fehler, R. Waltrich, E. S. Steiger, S. Häußler, P. Reddy, L. F. Kulikova, V. A. Davydov, V. N. Agafonov, M. W. Doherty, and A. Kubanek, Prolonged Orbital Relaxation by Locally Modified Phonon Density of States for the SiV- Center in Nanodiamonds, *Physical Review Letters* **128**, 153602 (2022).
- [22] R. Albrecht, A. Bommer, C. Deutsch, J. Reichel, and C. Becher, Coupling of a Single Nitrogen-Vacancy Center in Diamond to a Fiber-Based Microcavity, *Physical Review Letters* **110**, 243602 (2013).
- [23] R. Albrecht, A. Bommer, C. Pauly, F. Mücklich, A. W. Schell, P. Engel, T. Schröder, O. Benson, J. Reichel, and C. Becher, Narrow-band single photon emission at room temperature based on a single nitrogen-vacancy center coupled to an all-fiber-cavity, *Applied Physics Letters* **105**, 073113 (2014).
- [24] H. Kaupp, T. Hümmer, M. Mader, B. Schleder, J. Benedikter, P. Haeusser, H.-C. Chang, H. Fedder, T. W. Hänsch, and D. Hunger, Purcell-Enhanced Single-Photon Emission from Nitrogen-Vacancy Centers Coupled to a Tunable Microcavity, *Physical Review Applied* **6**, 054010 (2016).
- [25] J. Benedikter, H. Kaupp, T. Hümmer, Y. Liang, A. Bommer, C. Becher, A. Krueger, J. M. Smith, T. W. Hänsch, and D. Hunger, Cavity-Enhanced Single-Photon Source Based on the Silicon-Vacancy Center in Diamond, *Physical Review Applied* **7**, 024031 (2017).
- [26] S. Häußler, J. Benedikter, K. Bray, B. Regan, A. Dietrich, J. Twamley, I. Aharonovich, D. Hunger, and A. Kubanek, Diamond photonics platform based on silicon vacancy centers in a single-crystal diamond membrane and a fiber cavity, *Physical Review B* **99**, 165310 (2019).
- [27] R. Høy Jensen, E. Janitz, Y. Fontana, Y. He, O. Gobron, I. P. Radko, M. Bhaskar, R. Evans, C. D. Rodríguez Rosenblueth, L. Childress, A. Huck, and U. Lund Andersen, Cavity-Enhanced Photon Emission from a Single Germanium-Vacancy Center in a Diamond Membrane, *Physical Review Applied* **13**, 064016 (2020).
- [28] L. Greuter, S. Strosielec, D. Najer, A. Ludwig, L. Duempelmann, D. Rohner, and R. J. Warburton, A small mode volume tunable microcavity: Development and characterization, *Applied Physics Letters* **105**, 121105 (2014).
- [29] E. Janitz, M. Ruf, M. Dimock, A. Bourassa, J. Sankey, and L. Childress, Fabry-Perot microcavity for diamond-based photonics, *Physical Review A* **92**, 043844 (2015).
- [30] S. Bogdanović, S. B. van Dam, C. Bonato, L. C. Coenen, A.-M. J. Zwerver, B. Hensen, M. S. Z. Liddy, T. Fink, A. Reiserer, M. Lončar, and R. Hanson, Design and low-temperature characterization of a tunable microcavity for diamond-based quantum networks, *Applied Physics Letters* **110**, 171103 (2017).
- [31] S. B. van Dam, M. Ruf, and R. Hanson, Optimal design of diamond-air microcavities for quantum networks using an analytical approach, *New Journal of Physics* **20**, 115004 (2018).
- [32] E. Janitz, M. K. Bhaskar, and L. Childress, Cavity quantum electrodynamics with color centers in diamond, *Optica* **7**, 1232 (2020).
- [33] S. Vadia, J. Scherzer, H. Thierschmann, C. Schäfermeier, C. Dal Savio, T. Taniguchi, K. Watanabe, D. Hunger, K. Karraï, and A. Högele, Open-Cavity in Closed-Cycle Cryostat as a Quantum Optics Platform, *PRX Quantum* **2**, 040318 (2021).
- [34] Y. Fontana, R. Zifkin, E. Janitz, C. D. Rodríguez Rosenblueth, and L. Childress, A mechanically stable and tunable cryogenic Fabry-Pérot microcavity, *Review of Scientific Instruments* **92**, 053906 (2021).
- [35] T. Ruelle, D. Jaeger, F. Fogliano, F. Braakman, and M. Poggio, A tunable fiber Fabry-Pérot cavity for hybrid optomechanics stabilized at 4 K, *Review of Scientific Instruments* **93**, 095003 (2022).
- [36] S. Flågan, D. Riedel, A. Javadi, T. Jakubczyk, P. Maletinsky, and R. J. Warburton, A diamond-confined open microcavity featuring a high quality-factor and a small mode-volume, *Journal of Applied Physics* **131**, 113102 (2022).
- [37] M. Salz, Y. Herrmann, A. Nadarajah, A. Stahl, M. Hettrich, A. Stacey, S. Praver, D. Hunger, and F. Schmidt-Kaler, Cryogenic platform for coupling color centers in diamond membranes to a fiber-based microcavity, *Applied Physics B* **126**, 131 (2020).
- [38] S. Bogdanović, M. S. Z. Liddy, S. B. van Dam, L. C. Coenen, T. Fink, M. Lončar, and R. Hanson, Robust nano-fabrication of an integrated platform for spin control in a tunable microcavity, *APL Photonics* **2**, 126101 (2017).
- [39] K. G. Fehler, L. Antoniuk, N. Lettner, A. P. Ovvyan, R. Waltrich, N. Gruhler, V. A. Davydov, V. N. Agafonov, W. H. P. Pernice, and A. Kubanek, Hybrid Quantum Photonics Based on Artificial Atoms Placed Inside One Hole of a Photonic Crystal Cavity, *ACS Photonics* **8**, 2635 (2021).
- [40] S. Häußler, L. Hartung, K. G. Fehler, L. Antoniuk, L. F. Kulikova, V. A. Davydov, V. N. Agafonov, F. Jelezko, and A. Kubanek, Preparing single SiV- center in nanodiamonds for external, optical coupling with access to all degrees of freedom, *New Journal of Physics* **21**, 103047 (2019).
- [41] P. R. Dolan, G. M. Hughes, F. Grazioso, B. R. Patton, and J. M. Smith, Femtoliter tunable optical cavity arrays, *Optics Letters* **35**, 3556 (2010).
- [42] H. Kelkar, D. Wang, D. Martín-Cano, B. Hoffmann, S. Christiansen, S. Götzinger, and V. Sandoghdar, Sensing Nanoparticles with a Cantilever-Based Scannable Optical Cavity of Low Finesse and Sub- $\lambda/3$  Volume, *Physical Review Applied* **4**, 054010 (2015).
- [43] P. R. Dolan, S. Adekanye, A. A. P. Trichet, S. Johnson, L. C. Flatten, Y. C. Chen, L. Weng, D. Hunger, H.-C. Chang, S. Castelletto, and J. M. Smith., Robust, tunable, and high purity triggered single photon source at room temperature using a nitrogen-vacancy defect in diamond

- in an open microcavity, *Optics Express* **26**, 7056 (2018).
- [44] E. Neu, D. Steinmetz, J. Riedrich-Möller, S. Gsell, M. Fischer, M. Schreck, and C. Becher, Single photon emission from silicon-vacancy colour centres in chemical vapour deposition nano-diamonds on iridium, *New Journal of Physics* **13**, 025012 (2011).
- [45] J. L. Zhang, S. Sun, M. J. Burek, C. Dory, Y.-K. Tzeng, K. A. Fischer, Y. Kelaita, K. G. Lagoudakis, M. Radulaski, Z.-X. Shen, N. A. Melosh, S. Chu, M. Lončar, and J. Vučković, Strongly Cavity-Enhanced Spontaneous Emission from Silicon-Vacancy Centers in Diamond, *Nano Letters* **18**, 1360 (2018).
- [46] S. Meesala, Y.-I. Sohn, B. Pingault, L. Shao, H. A. Atikian, J. Holzgrafe, M. Gündoğan, C. Stavrakas, A. Sipahigil, C. Chia, R. Evans, M. J. Burek, M. Zhang, L. Wu, J. L. Pacheco, J. Abraham, E. Bielejec, M. D. Lukin, M. Atatüre, and M. Lončar, Strain engineering of the silicon-vacancy center in diamond, *Physical Review B* **97**, 205444 (2018).
- [47] L. J. Rogers, K. D. Jahnke, M. H. Metsch, A. Sipahigil, J. M. Binder, T. Teraji, H. Sumiya, J. Isoya, M. D. Lukin, P. Hemmer, and F. Jelezko, All-Optical Initialization, Readout, and Coherent Preparation of Single Silicon-Vacancy Spins in Diamond, *Physical Review Letters* **113**, 263602 (2014).
- [48] L. Rondin, J.-P. Tetienne, T. Hingant, J.-F. Roch, P. Maletinsky, and V. Jacques, Magnetometry with nitrogen-vacancy defects in diamond, *Reports on Progress in Physics* **77**, 056503 (2014).
- [49] V. Stepanov, F. H. Cho, C. Abeywardana, and S. Takahashi, High-frequency and high-field optically detected magnetic resonance of nitrogen-vacancy centers in diamond, *Applied Physics Letters* **106**, 063111 (2015).
- [50] P. van Loock, W. Alt, C. Becher, O. Benson, H. Boche, C. Deppe, J. Eschner, S. Höfling, D. Meschede, P. Michler, F. Schmidt, and H. Weinfurter, Extending Quantum Links: Modules for Fiber- and Memory-Based Quantum Repeaters, *Advanced Quantum Technologies* **3**, 1900141 (2020).
- [51] Y. Lee, E. Bersin, A. Dahlberg, S. Wehner, and D. Englund, A quantum router architecture for high-fidelity entanglement flows in quantum networks, *npj Quantum Information* **8**, 1 (2022).
- [52] J. M. Binder, A. Stark, N. Tomek, J. Scheuer, F. Frank, K. D. Jahnke, C. Müller, S. Schmitt, M. H. Metsch, T. Unden, T. Gehring, A. Huck, U. L. Andersen, L. J. Rogers, and F. Jelezko, Qudi: A modular python suite for experiment control and data processing, *SoftwareX* **6**, 85 (2017).